Physics Letters B 819 (2021) 136423

Contents lists available at ScienceDirect

Physics Letters B

www.elsevier.com/locate/physletb

Anisotropic quark stars in Einstein-Gauss-Bonnet theory

Takol Tangphati [a], Anirudh Pradhan [b], Abdelghani Errehymy [c,*], Ayan Banerjee [d]

[a] Department of Physics, Faculty of Science, Chulalongkorn University, Bangkok 10330, Thailand
[b] Department of Mathematics, Institute of Applied Sciences and Humanities, GLA University, Mathura, 281 406, Uttar Pradesh, India
[c] Laboratory of High Energy Physics and Condensed Matter (LPHEMaC), Department of Physics, Faculty of Sciences Aïn Chock, Hassan II University of Casablanca, B.P. 5366 Maarif, Casablanca 20100, Morocco
[d] Astrophysics and Cosmology Research Unit, School of Mathematics, Statistics and Computer Science, University of KwaZulu–Natal, Private Bag X54001, Durban 4000, South Africa

ARTICLE INFO

Article history:
Received 27 February 2021
Received in revised form 21 May 2021
Accepted 31 May 2021
Available online 3 June 2021
Editor: N. Lambert

ABSTRACT

Recent progress in the determination of both masses and radii of neutron stars has put strong constraints on the equation of state (EoS) above the nuclear saturation density. Within a confining quark matter model, we propose an anisotropic star consisting of a homogeneous and unpaired charge-neutral 3-flavor interacting quark matter with $\mathcal{O}(m_s^4)$ corrections in the context of Einstein-Gauss-Bonnet gravity theory. This generalized model depends only on three free parameters: the bag constant B, the interaction parameter a and the Gauss-Bonnet coupling constant α. Given the underlying EoS, we show the possibility of obtaining the maximal neutron star mass which satisfies the recent observational data for PSR J0751+1807. The numerical analysis of mass-radius relations supports the existence of other massive pulsars with a maximum mass consistent and common radii in the range of $R \lesssim (11 \sim 14)$ Km [1]. Furthermore, we discuss the mass vs central mass density ($M - \rho_c$) relation for stability, compactness and binding energy in this gravity theory. Our results thus provide circumstantial evidence in favor of super-massive pulsars in EGB gravity.

1. Introduction

A natural generalization of Einstein's general relativity (GR hereafter) is the Lovelock gravity. Lovelock gravity is the most general torsionless theory of gravity yielding conserved second order equations of motion in higher dimensions. This theory was originally introduced by Lanczos [2] in the year 1930, and rediscovered by David Lovelock [3]. This theory obeys generalized Bianchi identities which ensure energy conservation i.e., $\Delta^\mu T_{\mu\nu} = 0$, and it is known to be free of ghosts [4,5]. Among the higher curvature gravities, Lovelock gravity shares a number of additional nice properties including Einstein gravity that are not enjoyed by any other theories. Since, we know that the polynomial form of the Lagrangian in Lovelock theories; the first two terms correspond to cosmological constant and the Einstein-Hilbert action, while the second order term is the Gauss-Bonnet (GB) Lagrangian, respectively. This is the simplest nontrivial modification of GR providing modified dynamics, and leads to the well-known theory of Einstein-Gauss-Bonnet (EGB) gravity. Thus, EGB gravity is a particular case of more general Lovelock gravity emerges as a low energy effective action of heterotic string theory [6,7]. A broad avenue followed by many cosmological studies which can lead to accelerating cosmological solutions, see Refs. [8–10] for reviews on this. However, to get a non-trivial contribution, one can generally associate the GB term with the scalar field [11,12].

For instance, within the frame of the EGB gravity, Boulware and Deser [13] have found the spherically symmetric static black hole solution. Concerning this, black hole solution with a source as a cloud of strings has been found within this framework [14,15]. Soon after, several authors explored exact black hole solutions and their interesting properties from different view point (see, e.g., Refs. [16–20]). In the same context, gravitational collapse of an incoherent spherical dust cloud [21–24], geodesic motion of a Boulware-Deser black hole space-time [25], radius of photon spheres [26] and regular black hole solutions [27] have been addressed. In particular, static and spherically symmetric asymptotically flat wormhole solutions were found in [28,29] for both 4D and higher dimensional EGB gravity theory.

Compact objects generally represent the remnants of the stellar core which are left after the supernovae explosion [30,31] or

* Corresponding author.
E-mail addresses: takoltang@gmail.com (T. Tangphati), pradhan.anirudh@gmail.com (A. Pradhan), abdelghani.errehymy@gmail.com (A. Errehymy), ayanbanerjeemath@gmail.com (A. Banerjee).

https://doi.org/10.1016/j.physletb.2021.136423

by the formation of a planetary nebula. The new accumulating data from X-ray satellites and its associated electromagnetic counterpart have placed constraints on the dense matter equation of state (EoS). Thus, compact objects have provide a natural laboratory to explore the composition and structure of dense matter physics [1,32–35]. Under such conditions, physicists predicted different types of exotic matter with large strangeness fraction such as hyperon matter, Bose-Einstein condensates of strange mesons and quark matter may occur in the cores of neutron stars (NSs). Thus, one may predict that there could be a phase transition from nuclear to quark matter [36,37] at very high density in their interiors. Such constituents soften the EoS at high densities and that could lead to characteristic back-bending phenomenon in the timing of spinning-down pulsars [38].

Another reason for studying dense matter physics is the recent discovery of pulsars like PSR J0751+1807 with $M = 2.1 \pm 0.2 M_{\odot}$ [39] and J0348+0432 with $M = 2.01 \pm 0.04 M_{\odot}$ [40] have set the strong constraints on various matter EoS for NSs. By extending our microscopic results for the EoS, quark matter is by assumption absolutely stable and true ground state of hadronic matter, see [41,42] for more. Therefore, the quark stars (QSs) consist of *strange matter hypothesis* offers a unique tool to address the challenge of understanding the phase transition in the dense quantum chromodynamics (QCD). The quark matter (strange matter) might contain roughly equal numbers of up, down, and strange quarks. In this direction, the MIT-Bag Model has proved to be very successful in the description of the quark confinement where each quarks moves freely in a spherically symmetric well of infinity depth (bag). Moreover, QCD suggests that quark matter might be in different color superconducting phases at high densities. The studies based on the MIT bag model indicate the existence of stable configurations of QSs with the Color-Flavor-Locked (CFL) phase has also been suggested and intensively investigated [43–47].

In most of the cases it is believed that stars are made of an isotropic fluid source, where the radial pressure P_r equals the tangential pressure P_T. However, theoretical advances in the last decades indicate that such assumption does not hold always. For such fluid configurations the anisotropy means that the pressure along the radial direction P_r is differed from the transverse pressure P_T. There are many reasons to consider anisotropic fluids as interior models for spherical symmetry fluid sphere such as boson stars [48], gravastars [49] and neutron stars [50]. The main reason behind their extreme internal density and strong gravity hints that anisotropy of pressures is present within such compact objects [51]. Interesting features of relativistic anisotropic sphere was first pointed out by Lemaître [52], in 1933. While interest in anisotropic compact objects has been rekindled by Bowers and Liang [53]. These developments culminated by analyzing changes in the surface redshift and gravitational mass by generalization of the equation of hydrostatic equilibrium.

Further, Ruderman [54] pointed out that nuclear matter tends to become anisotropic at very high densities larger than 10^{15} g/cm^3. Letelier [55] showed that the energy-momentum tensor associated with the sum of two perfect fluids, one perfect and one null fluid, can give rise to anisotropic fluids. In the context of anisotropic stars, two-fluid dark matter models have studied [56] in General Relativity. In [57] authors have studied all static spherically symmetric anisotropic solutions. A nice study describing an exact solution of Einstein's field equations can be found in [58,59,74]. In addition, minimal gravitational decoupling (MGD) technique has widely been used to find exact solutions for self-gravitating systems, see for instance [60–64]. In [65] authors have introduced a covariant framework to study anisotropic stars in GR.

Motivated by the current achievements for anisotropic compact objects in GR, researchers have extended their solutions to the modified gravity theories [66,67]. An interesting result of this analysis is that static NSs have been found within the framework of R^2 gravity [68] (see, e.g., Refs. [69,70] for more). Addressing the problem of QSs in $4D$ EGB gravity [71], in comparison with GR, the present paper is devoted to explore anisotropic quark stars in the framework of EGB gravity. However, authors emphasized that investigations of the structure of QSs were carried out under the assumption of an isotropic perfect fluid EoS [71]. In fact, $4D$ EGB gravity has received several criticisms, including the above limiting procedure being invalid [72,73]. Thus, we decide to extend the solution describing a static spherically symmetric anisotropic quark matter distribution within the EGB gravity. Moreover, we would like to explore whether it is possible to have stellar structure in this context as well.

Furthermore, it is clear from observed pulsars that the NSs and their layers, one should not discard the existence of more exotic objects. As a consequence the fluid anisotropy may lead to significant changes in the characteristics of relativistic stars, as demonstrated in Refs. [74–76]. All the above arguments inspired us to perform a general analysis of physical viability and stability of anisotropic solutions for static QSs. Our purpose is to construct objects whose characteristics would be consistent with the current observational data like PSR J0348+0432 [40], PSR J0751+1807 [39], PSR J1903+0327 [77] and PSR J0437-4715 [78].

The present paper is organized as follows: The EGB gravity theory is briefly presented in Section 2. In this section, we write down the structure equations describing the star interior in EGB gravity. In Section 3, we present an overview of a QCD motivated EoS. Using these equations, in Section 4, we numerically find static solutions describing equilibrium configurations. Section 5 is devoted to analyze the mass-radius diagrams depending on the choice of various parameters in our proposed EGB gravity. In the next two Sections 6 and 7, we discuss the dynamical stability as well as other properties of QSs, such as compactness and binding energy. Finally we give our conclusions in section 8.

2. Basic equations of EGB gravity

The D-dimensional action for Einstein-Gauss-Bonnet (EGB) gravity with matter field reads:

$$\mathcal{I}_G = \frac{c^4}{16\pi G}\int d^D x\sqrt{-g}\,[R - 2\Lambda + \alpha\mathcal{L}_{\rm GB}] + \mathcal{S}_{\rm matter}, \tag{1}$$

where R and Λ are D-dimensional Ricci scalar and the cosmological constant, respectively. With $\mathcal{S}_{\rm matter}$ denotes the action associated with matter. The coupling constant α is of dimension [length]^2. A notable point is that α associates with the inverse string tension and positive definite. In particular, compact stars in Einstein-Dilaton-Gauss-Bonnet (EDGB) gravity have been studied for $\alpha > 0$ [79]. Thus, we shall restrict our study to the case of positive α. The Gauss-Bonnet Lagrangian $\mathcal{L}_{\rm GB}$ is the specific combination of Ricci scalar, Ricci tensor, and Riemann curvatures, and it is given by

$$\mathcal{L}_{\rm GB} = R^{\mu\nu\rho\sigma}R_{\mu\nu\rho\sigma} - 4R^{\mu\nu}R_{\mu\nu} + R^2. \tag{2}$$

Now, variation of the action (1) with respect to $g_{\mu\nu}$, one obtains the field equations

$$G_{\mu\nu} + \alpha H_{\mu\nu} = \frac{8\pi G}{c^4}T_{\mu\nu}\,, \quad \text{with} \quad T_{\mu\nu} = -\frac{2}{\sqrt{-g}}\frac{\delta\left(\sqrt{-g}\mathcal{S}_m\right)}{\delta g^{\mu\nu}}, \tag{3}$$

where $G_{\mu\nu}$ is the Einstein tensor and $H_{\mu\nu}$ is the contribution of the GB term with the following expression

$$G_{\mu\nu} = R_{\mu\nu} - \frac{1}{2} R\, g_{\mu\nu},$$
$$H_{\mu\nu} = 2\Big(R R_{\mu\nu} - 2R_{\mu\sigma} R^{\sigma}{}_{\nu} - 2R_{\mu\sigma\nu\rho} R^{\sigma\rho} - R_{\mu\sigma\rho\delta} R^{\sigma\rho\delta}{}_{\nu} \Big) - \frac{1}{2}\, g_{\mu\nu}\, \mathcal{L}_{\rm GB}. \tag{4}$$

Since the GB term is a topological invariant in $4D$ and thus it does not contribute to the field equations. To obtain compact strange stars, we write down the line element for static and spherically symmetric metric anstaz in D-dimensional, which is

$$ds_D^2 = -e^{2\Phi(r)} c^2 dt^2 + e^{2\lambda(r)} dr^2 + r^2 d\Omega_{D-2}^2, \tag{5}$$

where $d\Omega_{D-2}^2$ is the metric on the unit $(D-2)$-dimensional sphere. Moreover, $\Phi(r)$ and $\lambda(r)$ are functions of r, only. We will consider the stress-energy tensor of a perfect fluid, such that

$$T_{\mu\nu} = (\epsilon + P) u_\nu u_\nu + P g_{\nu\nu}, \tag{6}$$

where $P = P(r)$ is the pressure, $\epsilon = \epsilon(r)$ is the energy density of matter, and u_ν is the contravariant D-velocity. Now, using the Eqs. (5), (6) and (3), the non-vanishing components for a static, spherically symmetric perfect-fluid star in EGB theory read:

$$\frac{2}{r}\frac{d\lambda}{dr} = e^{2\lambda}\left[\frac{2}{(D-2)}\frac{8\pi G}{c^4}\epsilon - \frac{1-e^{-2\lambda}}{r^2}\left((D-3) + \frac{\alpha(D-5)(1-e^{-2\lambda})}{r^2}\right)\right] \times \left[1 + \frac{2\alpha(1-e^{-2\lambda})}{r^2}\right]^{-1}, \tag{7}$$

$$\frac{2}{r}\frac{d\Phi}{dr} = e^{2\lambda}\left[\frac{2}{(D-2)}\frac{8\pi G}{c^4}P + \frac{1-e^{-2\lambda}}{r^2}\left((D-3) + \frac{\alpha(D-5)(1-e^{-2\lambda})}{r^2}\right)\right] \times \left[1 + \frac{2\alpha(1-e^{-2\lambda})}{r^2}\right]^{-1}, \tag{8}$$

$$\frac{dP}{dr} = -(\epsilon + P)\frac{d\Phi}{dr} + \frac{3}{r}(P_\perp - P). \tag{9}$$

Since, we know that the higher order terms make a nonzero contribution in the field equation only for $D \geq 5$. Thus, we concentrate on $5D$ spherically symmetric star solution for the EGB gravity.

To study the general structure of the solution, we substitute by $e^{-2\lambda} = 1 - \frac{2Gm(r)}{c^2 r}$ the gravitational mass within the sphere of radius r. Using this we are in a position to write down the Tolman-Oppenheimer-Volkoff (TOV) equations in a convenient form. Finally, the conservation Eq. (9) has the following form

$$\frac{dP}{dr} = -\frac{2G\epsilon(r)m(r)}{c^2 r^2}\frac{\left[1 + \frac{P(r)}{\epsilon(r)}\right]\left[1 + \frac{4}{3}\frac{\pi r^3 P(r)}{c^2 m(r)}\right]}{\left[1 + \frac{4G\alpha m(r)}{c^2 r^3}\right]\left[1 - \frac{2Gm(r)}{c^2 r}\right]} + \frac{3}{r}(P_\perp(r) - P(r)). \tag{10}$$

The above equations are the modified TOV equations for $5D$ EGB gravity, and reduce to the standard TOV equations of GR when $\alpha \to 0$. Eq. (7) can be rewritten in terms of the mass parameter $m(r)$ as

$$m'(r) = \frac{-3c^2 r^3 m(r) + 12\alpha G m(r)^2 + 8\pi r^6 \epsilon(r)}{3\left(c^2 r^4 + 4\alpha G r m(r)\right)}, \tag{11}$$

where the prime denotes differentiation with respect to r. Before proceeding further, let us introduce the dimensionless quantities $P(r) = \epsilon_0 \bar{P}(r)$, $\epsilon(r) = \epsilon_0 \bar{\epsilon}(r)$ and $m(r) = M_\odot \bar{M}(r)$, with $\epsilon_0 = 1$ MeV/fm^3. Using these dimensionless parameters the above two equations become

$$\frac{d\bar{P}(r)}{dr} = -\frac{2c_1 \bar{\epsilon}(r)\bar{M}(r)}{r^2}\frac{\left[1 + \frac{\bar{P}(r)}{\bar{\epsilon}(r)}\right]\left[1 + \frac{c_2 r^3 \bar{P}(r)}{3\bar{M}(r)}\right]}{\left[1 + \frac{4c_1\alpha\bar{M}(r)}{r^3}\right]\left[1 - \frac{2c_1\bar{M}(r)}{r}\right]} + \frac{3}{r}\left(\bar{P}_\perp(r) - \bar{P}(r)\right), \tag{12}$$

and

$$\frac{d\bar{M}(r)}{dr} = \frac{-3r^3\bar{M}(r) + 12c_1\alpha\bar{M}(r)^2 + 2c_2 r^6 \bar{\epsilon}(r)}{3(r^4 + 4c_1\alpha r\bar{M}(r))}, \tag{13}$$

where $c_1 \equiv \frac{GM_\odot}{c^2} = 1.474$ km and $c_2 \equiv \frac{4\pi\epsilon_0}{M_\odot c^2} = 1.125 \times 10^{-5}$ km^{-3}. Thus closing the system, the matter EoS must be supplied. In the next section we will discuss QCD motivated EoS that represents a quark star interior solutions. We focus in detail on the question of how quark matter appears in compact stars, and how it affects the $M - R$ relations.

3. Interacting quark matter equation of state

In this section we introduce the EoS that we are going to use in our calculations for quark stars. Here we will discuss the structure equations representing QSs made of interacting quark matter. Depending on the density reached at the core of NS, different phases could be realized. We know that if the nuclear matter is compressed to sufficiently high density (beyond nuclear density which is around $\sim 10^{15}$ g/cm^3), then there is a phase transition from nuclear matter to quark matter. Such transitions have received much attention in those highly dense cores of NSs which lead to provide a unique environment to study cold matter at supernuclear densities. According to the hypothesis by Witten [41] cold strange quark matter could be absolutely stable, and this phase transition would favor the creation of a quark-matter phase over the entire star, so-called *strange stars* [36,37]. This so-called quark matter consists of almost equal amounts of up, down and strange quarks, and a small number of electrons to attain the charge neutrality.

As a result, the EoS concerning the strange quark matter (SQM) inspire the MIT-Bag model as a free Fermi gas of quarks. The MIT-Bag Model has become very popular in the study of SQM in astrophysics because of its simplicity. Nevertheless, the present knowledge of QCD suggests that quark stars are not such simple objects that depend only on the bag constant B at high densities. Thus, physicists predict several models based on QCD corrections of second and fourth order with the aim of giving an approximate characterization of confined quarks [80]. Here, we would like to employ the recently developed homogeneous and unpaired charge neutral 3-flavor interacting quark matter EoS [80]. For simplicity, we describe this phase using the simple thermodynamic Bag model EoS [81] with $\mathcal{O}(m_s^4)$ corrections. For example, several models predict the existence of QSs made of interacting quark EoS at ultra-high densities, as shown in Refs. [71,82]. Finally, the interacting quark EoS reads [82]

$$P = \frac{1}{3}(\epsilon - 4B) - \frac{m_s^2}{3\pi}\sqrt{\frac{\epsilon - B}{a_4}} + \frac{m_s^4}{12\pi^2}\left[1 - \frac{1}{a_4} + 3\ln\left(\frac{8\pi}{3m_s^2}\sqrt{\frac{\epsilon - B}{a_4}}\right)\right], \tag{14}$$

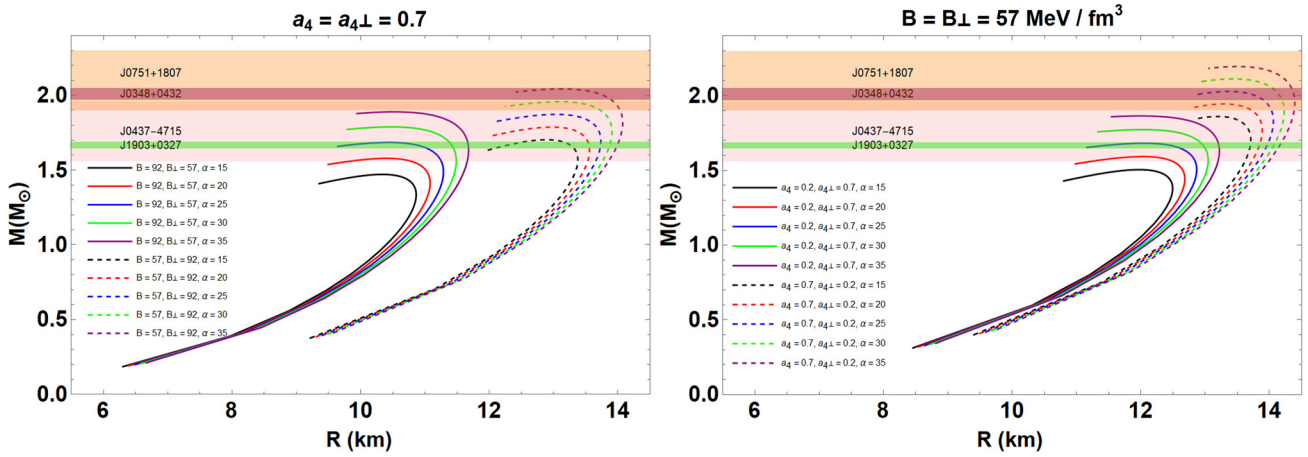

Fig. 1. Mass-Radius profile for $B \neq B_\perp$ (left panel) and $a_4 \neq a_4^\perp$ (right panel). We have plotted all graphs for different values of α as seen from the figure legends. The horizontal bands show the observational constraints from various pulsar measurements: PSR J0348+0432 (Purple) [40], PSR J0751+1807 (Orange) [39], PSR J0437-4715 (Pink) [78] and PSR J1903+0327 (Green) [77].

where ϵ is the energy density of homogeneously distributed quark matter (also to $\mathcal{O}(m_s^4)$ in the Bag model). As argued in [83], the strange quark mass is m_s to be 100 MeV [83] for our entire calculations and the Bag constant B lies in the range $57 \leq B \leq 92$ MeV/fm^3 [84,85]. Since the parameter a_4 comes from the QCD corrections on the pressure of the quark-free Fermi sea; vary within $0 < a_4 \leq 1$.

In this article we are dealing with anisotropic star, and thus the newly proposed generalized EoS for the tangential pressure followed by [82]:

$$
\begin{aligned}
P_\perp = P_c &+ \frac{1}{3}(\epsilon - 4B_\perp) - \frac{m_s^2}{3\pi}\sqrt{\frac{\epsilon - B_\perp}{a_4^\perp}} \\
&+ \frac{m_s^4}{12\pi^2}\left[1 - \frac{1}{a_4^\perp} + 3\ln\left(\frac{8\pi}{3m_s^2}\sqrt{\frac{\epsilon - B_\perp}{a_4^\perp}}\right)\right] \\
&- \frac{1}{3}(\epsilon_c - 4B_\perp) + \frac{m_s^2}{3\pi}\sqrt{\frac{\epsilon_c - B_\perp}{a_4^\perp}} \\
&- \frac{m_s^4}{12\pi^2}\left[1 - \frac{1}{a_4^\perp} + 3\ln\left(\frac{8\pi}{3m_s^2}\sqrt{\frac{\epsilon_c - B_\perp}{a_4^\perp}}\right)\right], \qquad (15)
\end{aligned}
$$

where ϵ_c and P_c are the central energy density and central radial pressure for Eq. (14), respectively. This ensures that at the center of the star the radial and tangential pressures are the same for $B = B_\perp$ and $a_4 = a_4^\perp$, which is desirable feature for any anisotropic fluid sphere. The parameters $a_4^\perp$ and $B_\perp$ associated with the expression for anisotropic pressure and vary in the same domain of a_4 and B.

4. Numerical results

The TOV equations consist of a system of ordinary differential equations that can be numerically integrated outwards from the origin ($r = 0$) to the point $r = R$ where the pressure becomes zero. The Eqs. (12) and (13) are solved with the help of EoSs (14) and (15), respectively. The solution of the above equations requires the following initial conditions $P(r_0) = P_c$ and $M(0) = 0$, where P_c is the central pressure. Varying P_c will thus give different masses and radii of the star. Note that we set $r_0 = 10^{-5}$ and mass $m(r_0) = 10^{-30}$ to avoid any kind of discontinuities that appear in the denominators. To synchronize each term given in Eqs. (14) and (15), we adopt the unit conversion 1 fm = 197.3 MeV.

Solving the equations by following procedure, we get a plot for the relation between the mass and radius of the QS. In our case, we focus our attention on $a_4 \neq a_4^\perp$ and $B \neq B_\perp$ i.e., complete anisotropic nature inside the stellar model. In addition, we vary the parameter $a_4^\perp$ from $0.1 \leq a_4^\perp \leq 0.9$, that relates to the maximum mass of the star around $2M_\odot$ at $a_4 \approx 0.7$, see Ref. [86]. The value of the central pressure of this model is $P(r_0) = 700$ MeV/fm^3 and the radius of the star is identified when the pressure vanishes or drops to a very small value. Moreover, the positive value of GB constant α has also been taken into consideration. The obtained maximum masses and corresponding radii will be summarized in the next section for QSs.

5. Mass-radius relation of an anisotropic quark star

The theoretical investigation of mass-radius relation for compact stars is important because those could be directly compared with measured masses and radii from various observations. For a given quark matter EoS, we need to find the mass-radius ($M - R$) relation depending on the choice of various parameters for spherically symmetric anisotropic quark star solutions. The main results of the computation depend on Eqs. (14) and (15), respectively.

Next, we move on to describe the results obtained from our calculations, which are illustrated in Fig. 1, for different values of α. In our analysis the choices of a_4, $a_4^\perp$, B and $B_\perp$ have significant impact on the mass radius relation as shown in the left and right panel of Fig. 1. Actually we represent four sets of ($M - R$) relation when $a_4 \neq a_4^\perp$ and $B \neq B_\perp$. This means we consider purely anisotropic interior solutions by considering four specific cases. It is also our main focus in this study of compact stars to achieve $\sim 2M_\odot$, which results from the recent constraints of massive pulsars measured today. This range of the $M_{\max}$ values covers well the observed pulsars like PSR J0348+0432 with $2.01 \pm 0.04 M_\odot$ (Purple) [40], PSR J0751+1807 with $2.1 \pm 0.2 M_\odot$ (Orange) [39], PSR J0437-4715 with $1.76 \pm 0.20 M_\odot$ (Pink) [78] and PSR J1903+0327 with $1.667 \pm 0.021\, M_\odot$ (Green) [77]. Based on this observation the categories can be defined as:

1. The mass-radius ($M - R$) relation depending on the choice of $B = 57$ and $B_\perp = 92$ with $a_4 = a_4^\perp = 0.7$ and progressively increasing values of α. In the left panel of Fig. 1 (dashed lines), each α produces a unique value of maximum mass. We can see a good agreement, represented by the magenta horizontal stripes, with some observed values for the mass of the pulsars ever detected, and calculated the maximum masses cor-

Table 1
Mass and radius of the maximum-mass stellar configuration for interacting quark matter EoS. Mass $M_{\max}$ is expressed in solar mass units, radius R is expressed in km, and the central energy density ϵ_c in MeV/fm^3. The numerical values are given for the case of $B \neq B_\perp$ and $a_4 = a_4^\perp$.

$a_4 = a_4^\perp$ (km^2)	B (MeV/fm^3)	$B_\perp$ (MeV/fm^3)	$M_{\max}$ ($M_\odot$)	R (km)	ϵ_c (MeV/fm^3)
0.1	57	57	1.93	11.90	5.29×10^3
		70	1.94	11.91	5.29×10^3
		92	1.94	11.90	5.35×10^3
0.5	70	57	1.96	11.82	5.25×10^3
		70	1.96	11.82	5.25×10^3
		92	1.96	11.81	5.31×10^3
0.7	92	57	1.89	10.58	7.92×10^3
		70	1.89	10.53	7.92×10^3
		92	1.89	10.53	7.92×10^3
0.9	92	57	1.89	10.58	7.79×10^3
		70	1.90	10.58	7.79×10^3
		92	1.90	10.58	7.79×10^3

responding to radii are tabulated in Table 1. For $\alpha = 35$ km^2, we recorded the maximum mass which yields $M_{\max} = 1.94 M_\odot$ with $R = 11.9$ km.

2. The second type of model comes from the choice of parameters $B = 92$ and $B_\perp = 57$ with $a_4 = a_4^\perp = 0.7$ in the left panel of Fig. 1 (solid lines). From this figure, one can see that there are significant differences for $M - R$ relation with respect to case 1. We see that maximum mass goes up to $M_{\max} = 1.89 M_\odot$ with $R = 10.58$ km, see Table 1.
3. Next, we consider the model for $a_4 = 0.7$ and $a_4^\perp = 0.2$ when $B = B_\perp = 57$. In the right panel of Fig. 1 (dashed lines), we plot $M - R$ graphs for different values α. We observe that the situation is completely different from the other two cases. In this scenario measured masses exceed $M_{\max} > 2M_\odot$, which correspond to maximum pulsar masses PSR J0348+0432 [40] and PSR J0751+1807 [39]. Within this EoS, $M_{\max}$ varies from ~ 2.38 to $\sim 2.02 M_\odot$, $R_{\max}$ ranges from ~ 13.57 to $\sim 13.06 M_\odot$ km.
4. Finally, we move on for $a_4 = 0.2$ and $a_4^\perp = 0.7$ when $B = B_\perp = 57$ (solid lines). Working under this hypothesis we have maximum masses $1.86 M_\odot$. Interestingly we observe that this situation is very similar to the first two cases. For the density regime $4.47 \times 10^3 \leq \epsilon_c$ (MeV/fm^3) $\leq 4.66 \times 10^3$ tabulated in Table 2.

Moreover, we recorded the values that cover a range of isotropic solution i.e., when $a_4 = a_4^\perp$ and $B = B_\perp$ in the Tables 1 and 2, respectively. Interestingly, we see from Tables 1 that anisotropy does not produce any significant effect with respect to the isotropic case, and all the solutions are overlapping each other. This situation is expected according to Ref. [82], though the solutions corresponding to GR. Surprisingly, we observe that one can distinguish the maximum mass found in Tables 2. We observe that the maximum masses of QSs for $a_4 > a_4^\perp$ are much larger than the ones determined in $a_4 < a_4^\perp$.

On the other hand, a profile of solutions that covers the full range of values for $B_\perp$ and $a_4^\perp$ is presented in Fig. 4. As it is clear from the Tables 1 that anisotropy does not produce any significant effect for $B \neq B_\perp$. But, it has significant influence on the maximum masses and radii. One can see from Fig. 4 that for less interacting quarks the maximum mass and their corresponding maximum radius have larger values. As an example, the combination $a_4 = 0.9$ and $a_4^\perp = 0.1$ give rise to a maximum mass $2.3 M_\odot$. Note that all figures have been plotted for $\alpha = 35$ km^2, as increasing values of α reach maximum masses faster.

Table 2
Numerical outcomes for maximum gravitational mass and its corresponding radius for $B = B_\perp$ and $a_4 \neq a_4^\perp$.

$B = B_\perp$ (MeV/fm^3)	a_4 (km^2)	$a_4^\perp$ (km^2)	$M_{\max}$ ($M_\odot$)	R (km)	ϵ_c (MeV/fm^3)	$2MG/Rc^2$	Z_{surf}
57	0.2	0.1	2.11	12.84	4.66×10^3	0.483	0.391
		0.2	1.98	12.49	4.60×10^3	0.468	0.371
		0.3	1.93	12.29	4.51×10^3	0.464	0.366
		0.5	1.89	12.11	4.47×10^3	0.460	0.360
		0.7	1.86	11.98	4.42×10^3	0.459	0.359
		0.9	1.84	11.91	4.40×10^3	0.458	0.358
57	0.7	0.1	2.38	13.57	5.35×10^3	0.516	0.441
		0.2	2.19	13.51	4.10×10^3	0.479	0.386
		0.3	2.13	13.35	3.85×10^3	0.470	0.374
		0.5	2.07	13.21	3.67×10^3	0.462	0.364
		0.7	2.04	13.12	3.60×10^3	0.458	0.359
		0.9	2.02	13.06	3.57×10^3	0.457	0.357
70	0.5	0.1	2.17	12.38	6.16×10^3	0.517	0.439
		0.2	2.05	12.10	5.43×10^3	0.500	0.414
		0.3	2.00	11.96	5.32×10^3	0.493	0.405
		0.5	1.96	11.82	5.25×10^3	0.488	0.398
		0.7	1.93	11.73	5.31×10^3	0.486	0.395
		0.9	1.92	11.68	5.27×10^3	0.486	0.393
92	0.9	0.1	2.09	11.15	8.39×10^3	0.552	0.494
		0.2	2.00	10.93	7.73×10^3	0.539	0.472
		0.3	1.96	10.82	7.70×10^3	0.534	0.465
		0.5	1.93	10.70	7.67×10^3	0.531	0.459
		0.7	1.91	10.63	7.63×10^3	0.529	0.457
		0.9	1.90	10.58	7.59×10^3	0.528	0.456

6. Dynamical stability of quark stars

We now proceed to study the stellar mass M against the central energy density ϵ_c for different values of GB constant α and for other parameters as indicated in the previous section. This fact justifies the wide use of the following static stability criterion instead of the dynamical one:

$$\frac{\partial M(\epsilon_c)}{\partial \epsilon_c} < 0 \implies \text{(unstable configuration)}, \tag{16}$$

$$\frac{\partial M(\epsilon_c)}{\partial \epsilon_c} > 0 \implies \text{(stable configuration)}. \tag{17}$$

In practice, this criterion is a necessary condition but not sufficient. In the Fig. 2, we plot M (in solar masses $M_\odot$) against ϵ_c for compact stars modeled by the interacting quark EoS. We use central energy densities in the range $500 \leq \epsilon_c \leq 6000$ MeV/fm^3. For this range of central pressures we observe that the mass of the star grows with the increment of the central energy density until it reaches a maximum mass in $\epsilon_c = \epsilon_c^*$. This means that $(M_{\max}, R_{M_{\max}})$ is a boundary separating the stable configuration region from the unstable one.

7. Compactness and binding energy

In this section we discuss the gravitational redshift [87] which is related to the emission produced by photons from the star surface, and defined by

$$Z_{\text{surf}} = \left(1 - r_g/R\right)^{-1/2} - 1, \tag{18}$$

where $r_g = 2GM/c^2$ and R is the radius of the star. Since, the compactness $2MG/Rc^2$ leads to the redshift value for the anisotropic solution which is compared with the isotropic case also. We explicitly compute the compactness for different values of bag constant. The maximum mass along with those compactness parame-

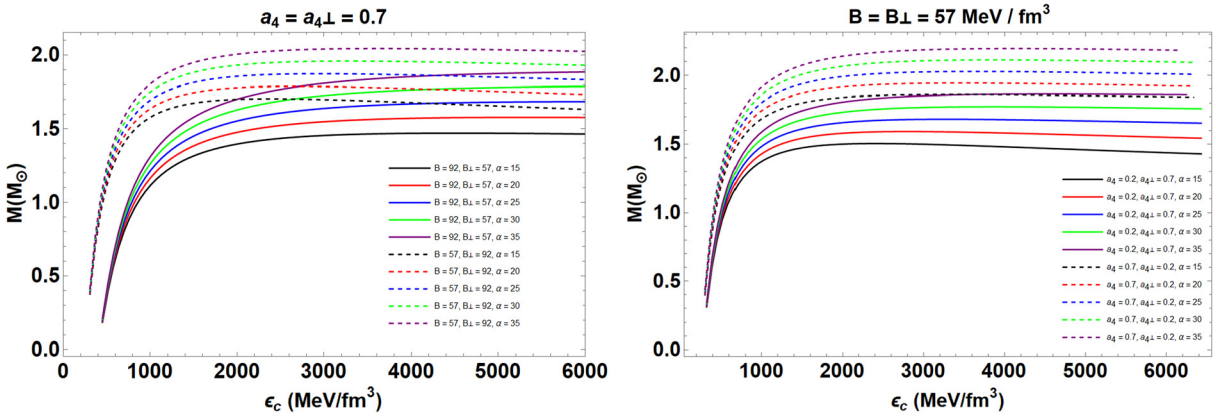

Fig. 2. The figure represents the relations between the total mass versus the central energy density of the QSs for the interacting quark matter model.

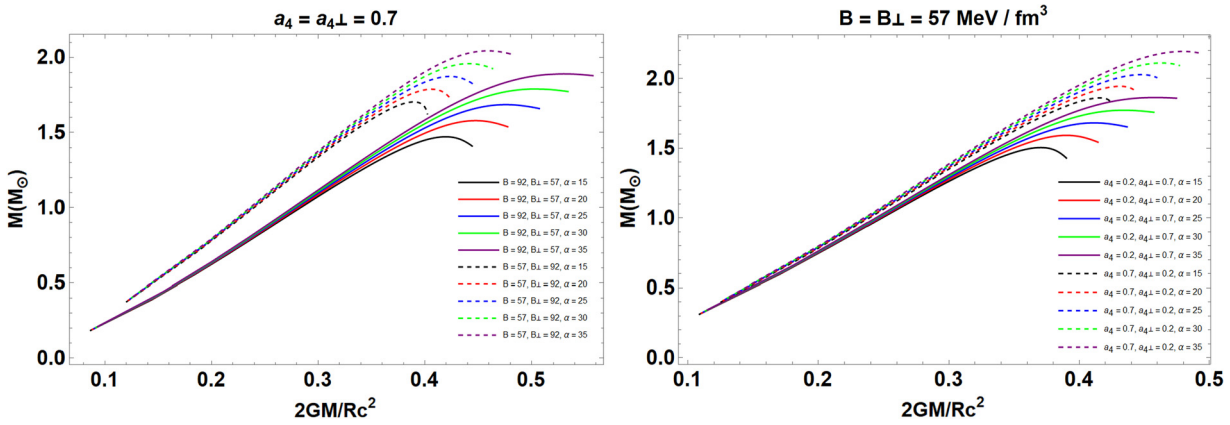

Fig. 3. Relations between maximum mass versus the $2GM/c^2R$ (compactness). In both figures, we have used $\alpha = 35$ to get the maximum effect on the star.

ter are displayed in Fig. 3 for different parameter sets. Observing the figures the trend of stellar compactness lies in the range of $0.45 < r_g/R < 0.56$. The numerical values given in Table 2. In contrast, $Z_{\rm surf}^{a_4=0.9} = 0.494$ corresponds to the most interacting quark matter and consequently the most compact quark star modeled for highest value of the bag parameter $B = B_\perp = 92$.

Our next step is to discussions on the gravitational binding energy E_g. We calculate E_g for all the permitted values of the bag constant and the interacting parameter. Having verified the full range of $B = B_\perp$, we vary $0 < a_4^\perp < 1$ for $a_4 = 0.1$, 0.5, 0.7 and 0.9, respectively. It is evident from the Fig. 5 that QSs reach the maximum binding energy when the difference between the a_4 and $a_4^\perp$ is much higher for the lowest bag parameter B. This result further indicates that the less interacting quarks have larger binding energy.

8. Concluding remarks

Investigating the properties of quark stars (QSs) have attracted much attention, because they are excellent laboratories for matter under extreme conditions. The structure of QSs depend mainly on the EoS used to describe their internal composition. In this work we have analyzed QSs assuming an interacting EoS with the bag constant B and the interaction parameter a, is fundamental for the construction of stable equilibrium solution. Considering anisotropic configuration of strange matter, we have integrated the TOV equations numerically to get the values of mass, radius and the other physical properties of the star. The resulting mass and radius is strictly dependent on the three parameters i.e., two parameters coming from the EoS under consideration, and another one is the GB coupling constant α coming from Einstein-Gauss-Bonnet (EGB) gravity. Since, the EGB gravity is a natural and most effective generalization of Einstein's general relativity, to higher dimensions.

Concerning the dependence of the physical properties of the QSs on the GB coupling constant α, we note that the maximum mass of QS increases to more than $2M_\odot$ for larger values of α. We mainly concentrated two sets of solution for (i) $a_4 = a_4^\perp$ when $B \neq B_\perp$ and (ii) $a_4 \neq a_4^\perp$ when $B = B_\perp$, where the anisotropy occurs at the level of the tangential component of the pressure. Then we varied the tangential components $a_4^\perp$ and $B_\perp$, while the radial composers a_4 and B are being fixed. We showed that, $B_\perp$ do not produce any significant effect with respect to the isotropic case. This situation can be seen clearly in Table 1 where we consider the numerical values for $a_4 = a_4^\perp$ and $B \neq B_\perp$. However, this situation is quite different when we consider the case for $a_4 \neq a_4^\perp$, see Table 2 for more details. We get the maximum effect on the mass-radius relation for lowest value of bag parameter $B = 57$ MeV/fm^3. Moreover, the values of interacting parameter a_4 in the physically expected range, in between $0 < a_4 < 1$, where one can get influence of strong interactions. Compared to the solution obtained in [71], it is evident that the obtained results are essentially model dependent and are in general determined by a specific type of EGB gravity.

Next, we examined the diagrams related to $M - \epsilon_c$, compactness and binding energy, respectively. We studied the stability of QSs by the following inequality $\frac{\partial M(\epsilon_c)}{\partial \epsilon_c} \lesseqgtr 0$, though it is a necessary condition for recognizing stable configurations. We show that the

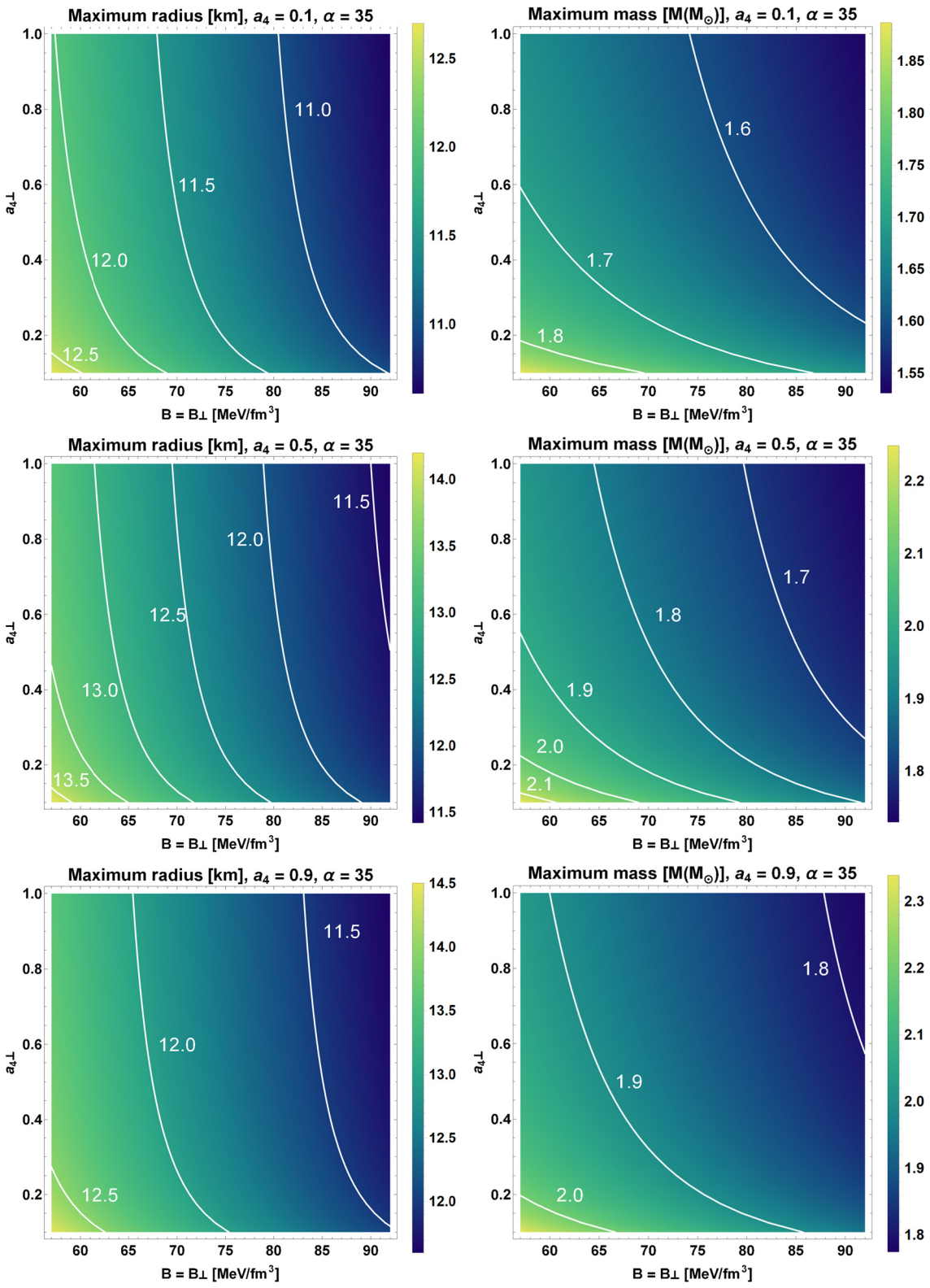

Fig. 4. Maximum masses and their corresponding radii for the full range of values of $B_\perp$ and $a_4^\perp$. The contour plot for $B = B_\perp$ with varying $a_4^\perp$ in the range of $0 < a_4^\perp < 1$ for $a_4 = 0.1$, 0.5 and 0.9, respectively.

binding energy increases monotonically for $a_4 = 0.1$ to $a_4 = 0.9$, but the trend is not linear. Moreover, less interacting quarks have larger binding energy. Thus, the presence of anisotropic quark matter distribution leads to considerable changes both in the structure of the stars and the mass-radius relation.

Declaration of competing interest

The authors declare that they have no known competing financial interests or personal relationships that could have appeared to influence the work reported in this paper.

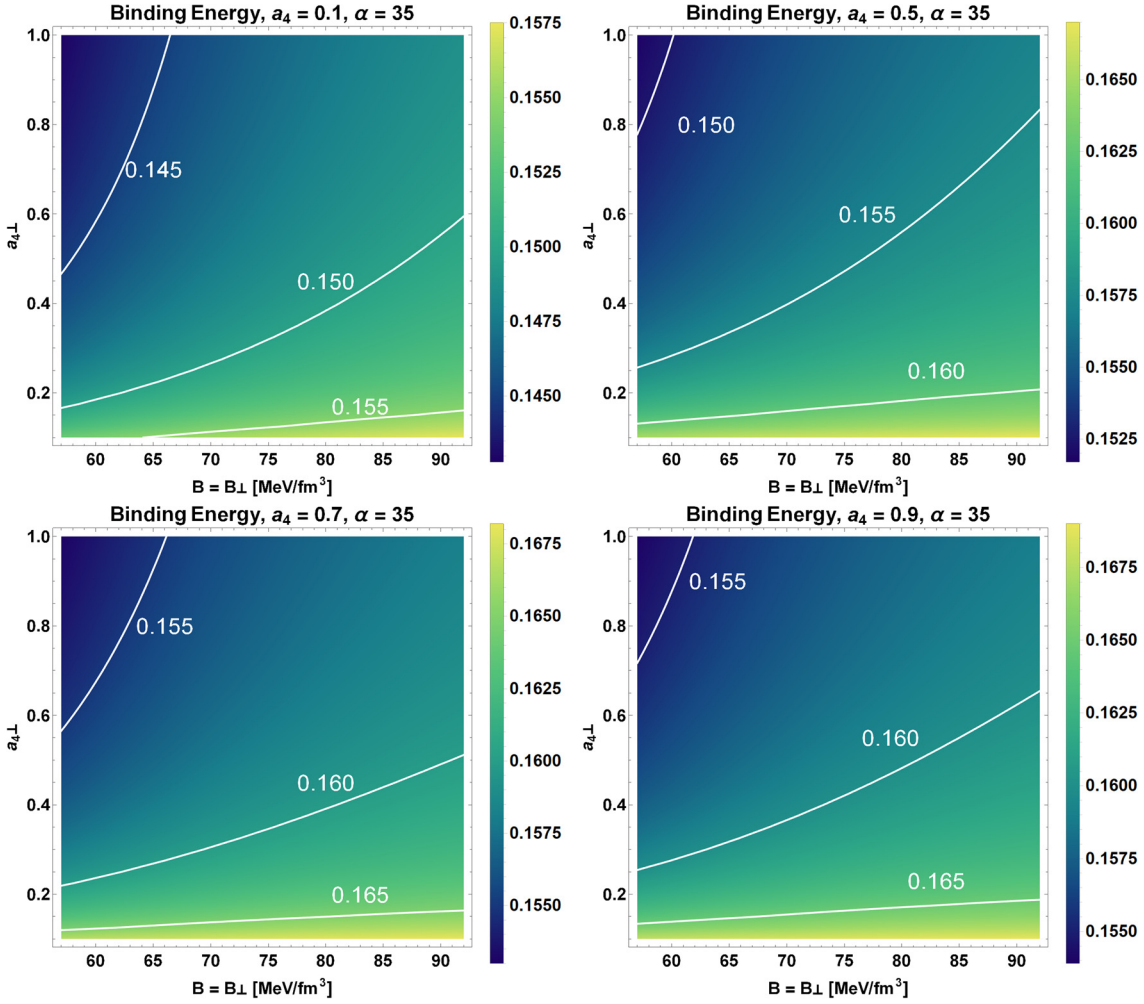

Fig. 5. Binding energy profile for the full range of values of $B_\perp$ and $a_4^\perp$. Each numerical values are given in Table 2.

Acknowledgements

The author TT would like to thank the financial support from the Science Achievement Scholarship of Thailand (SAST).

References

[1] A.W. Steiner, J.M. Lattimer, E.F. Brown, Astrophys. J. 722 (2010) 33.
[2] C. Lanczos, Ann. Math. 39 (1938) 842.
[3] D. Lovelock, J. Math. Phys. 12 (1971) 498;
D. Lovelock, J. Math. Phys. 13 (1972) 874.
[4] B. Zwiebach, Phys. Lett. B 156 (1985) 315.
[5] B. Zumino, Phys. Rep. 137 (1986) 109.
[6] D.L. Wiltshire, Phys. Lett. B 169 (1986) 36.
[7] J.T. Wheeler, Nucl. Phys. B 268 (1986) 737.
[8] S. Nojiri, S.D. Odintsov, V.K. Oikonomou, Phys. Rev. D 99 (2019) 044050.
[9] S. Nojiri, S.D. Odintsov, V.K. Oikonomou, N. Chatzarakis, T. Paul, Eur. Phys. J. C 79 (2019) 565.
[10] S.D. Odintsov, V.K. Oikonomou, Phys. Lett. B 797 (2019) 134874.
[11] S.D. Odintsov, V.K. Oikonomou, Phys. Lett. B 805 (2020) 135437.
[12] S.D. Odintsov, V.K. Oikonomou, F.P. Fronimos, Nucl. Phys. B 958 (2020) 115135.
[13] D.G. Boulware, S. Deser, Phys. Rev. Lett. 55 (1985) 2656.
[14] E. Herscovich, M.G. Richarte, Phys. Lett. B 689 (2010) 192.
[15] S.H. Mazharimousavi, M. Halilsoy, Phys. Lett. B 681 (2009) 190.
[16] S.G. Ghosh, M. Amir, S.D. Maharaj, Eur. Phys. J. C 77 (2017) 530.
[17] D. Rubiera-Garcia, Phys. Rev. D 91 (2015) 064065.
[18] A. Giacomini, J. Oliva, A. Vera, Phys. Rev. D 91 (2015) 104033.
[19] L. Aranguiz, X.M. Kuang, O. Miskovic, Phys. Rev. D 93 (2016) 064039.
[20] W. Xu, J. Wang, X.h. Meng, Phys. Lett. B 742 (2015) 225.
[21] S. Jhingan, S.G. Ghosh, Phys. Rev. D 81 (2010) 024010.
[22] H. Maeda, Phys. Rev. D 73 (2006) 104004.
[23] K. Zhou, Z.Y. Yang, D.C. Zou, R.H. Yue, Mod. Phys. Lett. A 26 (2011) 2135.
[24] G. Abbas, M. Zubair, Mod. Phys. Lett. A 30 (2015) 1550038.
[25] B. Bhawal, Phys. Rev. D 42 (1990) 449.
[26] E. Gallo, J.R. Villanueva, Phys. Rev. D 92 (2015) 064048.
[27] S.G. Ghosh, D.V. Singh, S.D. Maharaj, Phys. Rev. D 97 (2018) 104050.
[28] H. Maeda, M. Nozawa, Phys. Rev. D 78 (2008) 024005.
[29] K. Jusufi, A. Banerjee, S.G. Ghosh, Eur. Phys. J. C 80 (2020) 698.
[30] S.E. Woosley, A. Heger, T.A. Weaver, Rev. Mod. Phys. 74 (2002) 1015.
[31] A. Heger, C.L. Fryer, S.E. Woosley, N. Langer, D.H. Hartmann, Astrophys. J. 591 (2003) 288.
[32] F. Weber, Pulsars as Astrophyical Laboratories for Nuclear and Particle Physics, IOP Publishing Ltd, London, 1999.
[33] N.K. Glendenning, Compact Stars, 2nd ed., Spinger-Verlag, New York, 2000.
[34] J.M. Lattimer, M. Prakash, Science 304 (2004) 536.
[35] A.W. Steiner, M. Prakash, J.M. Lattimer, P.J. Ellis, Phys. Rep. 411 (2005) 325.
[36] C. Alcock, E. Farhi, A.V. Olinto, Astrophys. J. 310 (1986) 261.
[37] P. Haensel, J. Zdunik, R. Schaeffer, Astron. Astrophys. 160 (1986) 121.
[38] N.K. Glendenning, S. Pei, F. Weber, Phys. Rev. Lett. 79 (1997) 1603.
[39] D.J. Nice, E.M. Splaver, I.H. Stairs, O. Loehmer, A. Jessner, M. Kramer, J.M. Cordes, Astrophys. J. 634 (2005) 1242.
[40] J. Antoniadis, P.C.C. Freire, N. Wex, et al., Science 340 (2013) 6131.
[41] E. Witten, Phys. Rev. D 30 (1984) 272.
[42] A.R. Bodmer, Phys. Rev. D 4 (1971) 1601.
[43] C.V. Flores, G. Lugones, Phys. Rev. C 95 (2017) 025808.
[44] C.V. Flores, G. Lugones, Phys. Rev. D 82 (2010) 063006.
[45] A. Banerjee, K.N. Singh, arXiv:2005.04028 [gr-qc].
[46] G. Lugones, J. Horvath, Astron. Astrophys. 403 (2003) 173.
[47] K.N. Singh, A. Banerjee, S.K. Maurya, F. Rahaman, A. Pradhan, Phys. Dark Universe 31 (2021) 100774.
[48] F.E. Schunck, E.W. Mielke, Class. Quantum Gravity 20 (2003) R301.
[49] C. Cattoen, T. Faber, M. Visser, Class. Quantum Gravity 22 (2005) 4189.
[50] H. Heintzmann, W. Hillebrandt, Astron. Astrophys. 38 (1975) 51.
[51] L. Herrera, N.O. Santos, Phys. Rep. 286 (1997) 53.
[52] G. Lemaître, Ann. Soc. Sci. Brux. A 53 (1933) 51.

[53] R.L. Bowers, E.P.T. Liang, Astrophys. J. 188 (1974) 657.
[54] R. Ruderman, Annu. Rev. Astron. Astrophys. 10 (1972) 427.
[55] P.S. Letelier, Phys. Rev. D 22 (1980) 807.
[56] T. Harko, F.S.N. Lobo, Phys. Rev. D 83 (2011) 124051.
[57] L. Herrera, J. Ospino, A. Di Prisco, Phys. Rev. D 77 (2008) 027502.
[58] S.K. Maurya, A. Banerjee, S. Hansraj, Phys. Rev. D 97 (2018) 044022.
[59] J.M.Z. Pretel, Eur. Phys. J. C 80 (2020) 726.
[60] M. Sharif, S. Sadiq, Eur. Phys. J. C 78 (2018) 410.
[61] L. Gabbanelli, Á. Rincón, C. Rubio, Eur. Phys. J. C 78 (2018) 370.
[62] S.K. Maurya, F. Tello-Ortiz, Eur. Phys. J. C 79 (2019) 85.
[63] R. Pérez Graterol, Eur. Phys. J. Plus 134 (2019) 369.
[64] K.N. Singh, S.K. Maurya, M.K. Jasim, F. Rahaman, Eur. Phys. J. C 79 (2019) 851.
[65] G. Raposo, P. Pani, M. Bezares, C. Palenzuela, V. Cardoso, Phys. Rev. D 99 (2019) 104072.
[66] D. Deb, F. Rahaman, S. Ray, B.K. Guha, Phys. Rev. D 97 (2018) 084026.
[67] I.G. Salako, M. Khlopov, S. Ray, M.Z. Arouko, P. Saha, U. Debnath, Universe 6 (2020) 167.
[68] V. Folomeev, Phys. Rev. D 97 (2018) 124009.
[69] S.D. Odintsov, V.K. Oikonomou, arXiv:2104.01982 [gr-qc].
[70] S.D. Odintsov, V.K. Oikonomou, Phys. Dark Universe 32 (2021) 100805.
[71] A. Banerjee, T. Tangphati, D. Samart, P. Channuie, Astrophys. J. 906 (2021) 114.
[72] H. Lu, Y. Pang, Phys. Lett. B 809 (2020) 135717.
[73] L. Ma, H. Lu, Eur. Phys. J. C 80 (2020) 1209.
[74] M.K. Mak, T. Harko, Proc. R. Soc. Lond. A 459 (2003) 393.
[75] D. Horvat, S. Ilijic, A. Marunovic, Class. Quantum Gravity 28 (2011) 025009.
[76] V. Folomeev, V. Dzhunushaliev, Phys. Rev. D 91 (2015) 044040.
[77] P.C.C. Freire, C.G. Bassa, N. Wex, et al., Mon. Not. R. Astron. Soc. 412 (2011) 2763.
[78] J.P.W. Verbiest, M. Bailes, W. van Straten, G.B. Hobbs, R.T. Edwards, R.N. Manchester, N.D.R. Bhat, J.M. Sarkissian, B.A. Jacoby, S.R. Kulkarni, Astrophys. J. 679 (2008) 675.
[79] P. Pani, E. Berti, V. Cardoso, J. Read, Phys. Rev. D 84 (2011) 104035.
[80] C.V. Flores, Z.B. Hall II, P. Jaikumar, Phys. Rev. C 96 (2017) 065803.
[81] M. Alford, M. Braby, M. Paris, S. Reddy, Astrophys. J. 629 (2005) 969.
[82] E.A. Becerra-Vergara, S. Mojica, F.D. Lora-Clavijo, A. Cruz-Osorio, Phys. Rev. D 100 (2019) 103006.
[83] J. Beringer, et al., Phys. Rev. D 86 (2012) 010001.
[84] G. Fiorella Burgio, A.F. Fantina, Astrophys. Space Sci. Libr. 457 (2018) 255.
[85] D. Blaschke, N. Chamel, Astrophys. Space Sci. Libr. 457 (2018) 337.
[86] E.S. Fraga, R.D. Pisarski, J. Schaffner-Bielich, Phys. Rev. D 63 (2001) 121702.
[87] P. Haensel, A.Y. Potekhin, D.G. Yakovlev, Neutron Stars 1: Equation of State and Structure, Springer-Verlag, New York, 2007.